© 2019. Published by The Company of Biologists Ltd | Journal of Cell Science (2019) 132, jcs231993. doi:10.1242/jcs.231993

SHORT REPORT

Yap induces osteoblast differentiation by modulating Bmp signalling during zebrafish caudal fin regeneration

Ana S. Brandão[1], Anabela Bensimon-Brito[2,*], Raquel Lourenço[1], Jorge Borbinha[1], Ana Rosa Soares[1], Rita Mateus[3] and António Jacinto[1,*]

ABSTRACT

Osteoblast differentiation is a key process for bone homeostasis and repair. Multiple signalling pathways have been associated with osteoblast differentiation, yet much remains unknown on how this process is regulated *in vivo*. Previous studies have proposed that the Hippo pathway transcriptional co-activators YAP and TAZ (also known as YAP1 and WWTR1, respectively) maintain progenitor stemness and inhibit terminal differentiation of osteoblasts, whereas others suggest they potentiate osteoblast differentiation and bone formation. Here, we use zebrafish caudal fin regeneration as a model to clarify how the Hippo pathway regulates *de novo* bone formation and osteoblast differentiation. We demonstrate that Yap inhibition leads to accumulation of osteoprogenitors and prevents osteoblast differentiation in a cell non-autonomous manner. This effect correlates with a severe impairment of Bmp signalling in osteoblasts, likely by suppressing the expression of the ligand *bmp2a* in the surrounding mesenchymal cells. Overall, our findings provide a new mechanism of bone formation through the Hippo–Yap pathway, integrating Yap in the signalling cascade that governs osteoprogenitor maintenance and subsequent differentiation during zebrafish caudal fin regeneration.

KEY WORDS: Bone, Hippo pathway, Regeneration, Paracrine signalling, Osteoblast

INTRODUCTION

Bone formation and repair are intrinsically associated with the balanced activity of bone-forming cells, the osteoblasts (Long, 2012). Dysfunctional behaviour of osteoblasts leads to improper bone matrix deposition and mineralization, affecting the size, shape and integrity of the skeletal structures (Valenti et al., 2017). Bone defects occur under pathological conditions (Corrado et al., 2017), or are due to defective healing upon infection or trauma (Dimitriou et al., 2011). Current strategies to augment bone formation, like autologous bone grafts (Shrivats et al., 2014) or the use of growth factors (El Bialy et al., 2017), show promising results. However, a better understanding of the osteoblast lineage specification and bone regeneration would considerably improve these therapeutic strategies.

Osteoblasts derive from osteoprogenitors that differentiate by progressively expressing maturation markers (Rutkovskiy et al., 2016). More immature cells express runt-related transcription factor 2 (*Runx2*) (Ducy et al., 1997), followed by osterix (*Osx*) (Nakashima et al., 2002) and, finally, the mature-osteoblast marker, bone γ-carboxyglutamate protein (*Bglap* or *Osteocalcin*) (Wei and Karsenty, 2015). The Hippo pathway has been recently suggested to mediate bone formation and repair by specifying the osteoblast lineage (Kegelman et al., 2018). This signal transduction pathway comprises a kinase core cascade which, when activated, leads to the phosphorylation, cytoplasm sequestration and degradation of its effectors, Yes-associated protein 1 (YAP, also known as YAP1) and transcriptional co-activator with PDZ-binding motif (TAZ, also known as WWTR1). When the Hippo cascade is inactive, YAP and TAZ translocate to the nucleus and regulate target gene expression (Irvine, 2012; Misra and Irvine, 2018). This pathway plays an important function in tissue growth, organ size and regeneration (Moya and Halder, 2019) by regulating cell proliferation, survival and fate determination (Yu and Guan, 2013). Recent works show that YAP and TAZ are required for proper osteoblast activity and bone formation *in vitro* (Halder et al., 2012), during mouse development and adult bone remodelling (Pan et al., 2018; Tang et al., 2013). However, their roles are still controversial and context dependent, maintaining self-renewal properties in osteoprogenitors, while promoting bone formation in mature osteoblasts (Seo et al., 2013; Xiong et al., 2018).

While mammals show limited ability to regenerate (Zhao et al., 2016), zebrafish (*Danio rerio*) can regrow multiple organs and tissues upon injury (Antos et al., 2016). Bone is a major tissue in the zebrafish caudal fin (Pfefferli and Jaźwińska, 2015) and its regeneration relies on dedifferentiation of mature osteoblasts and on the recruitment of resident progenitor cells (Ando et al., 2017; Sousa et al., 2011), which assemble an osteoprogenitor pool. These osteoprogenitors differentiate into mature osteoblasts that produce the new mineralized bone (Wehner and Weidinger, 2015). We have previously shown that the Hippo pathway, through its effector Yap, regulates early stages of caudal fin regeneration by controlling cell proliferation (Mateus et al., 2015). Here, we reveal a novel role for Yap in promoting pivotal cell fate decisions during caudal fin regeneration. Our results show that Yap activity in mesenchymal cells induces, via a paracrine mechanism, the activation of Bmp signalling in osteoblasts, thereby dictating the initiation of osteoblast differentiation.

RESULTS AND DISCUSSION

Yap inhibition results in major bone defects during caudal fin regeneration

In zebrafish, after caudal fin amputation, mature cells re-enter the cell cycle and form a less-differentiated, proliferative and lineage-restricted pool of cells (Tu and Johnson, 2011), called a blastema;

[1]CEDOC, NOVA Medical School, NOVA University of Lisbon, Campo Mártires da Pátria 130, Lisboa 1169-056, Portugal. [2]Department of Developmental Genetics, Max Planck Institute for Heart and Lung Research, 61231 Bad Nauheim, Germany. [3]Department of Biochemistry, Sciences II, University of Geneva, Quai Ernest-Ansermet 30, 1211 Geneva 4, Switzerland.

*Authors for correspondence (anabela.bensimon-brito@mpi-bn.mpg.de; antonio.jacinto@nms.unl.pt)

A.S.B., 0000-0001-5842-033X; A.B.-B., 0000-0003-1663-2232; R.L., 0000-0002-6176-3066; J.B., 0000-0003-0720-5642; A.R.S., 0000-0002-0371-4610; R.M., 0000-0002-6023-3880; A.J., 0000-0002-4193-6089

Received 13 March 2019; Accepted 14 October 2019

Journal of Cell Science (2019) 132, jcs231993. doi:10.1242/jcs.231993

this group of cells will reconstitute the regenerated tissue (Kawakami, 2010; Poss et al., 2003). After blastema formation and outgrowth initiation, differentiation of new osteoblasts takes place, culminating in bone matrix deposition and patterning of new bony-rays (Marí-Beffa and Murciano, 2010). To determine whether Yap controls bone formation during caudal fin regeneration, we used a heat-shock transgenic line expressing a dominant-negative form of Yap, *hsp70*:RFP-DNyap (referred to hereafter as DN-Yap+) (Mateus et al., 2015). Although homozygous viable mutants for *yap1* are available (Kimelman et al., 2017), the heat-shock inducible strategy allows us to address the role of Yap in a time-specific manner, without affecting blastema formation. Therefore, to determine the effect of Yap inhibition during bone formation, we subjected DN-Yap+ and DN-Yap− siblings to two experimental protocols (Fig. 1A,B). First, a short Yap inhibition assay, consisting of a single heat-shock at 48 h post-amputation (hpa) and fin analysis

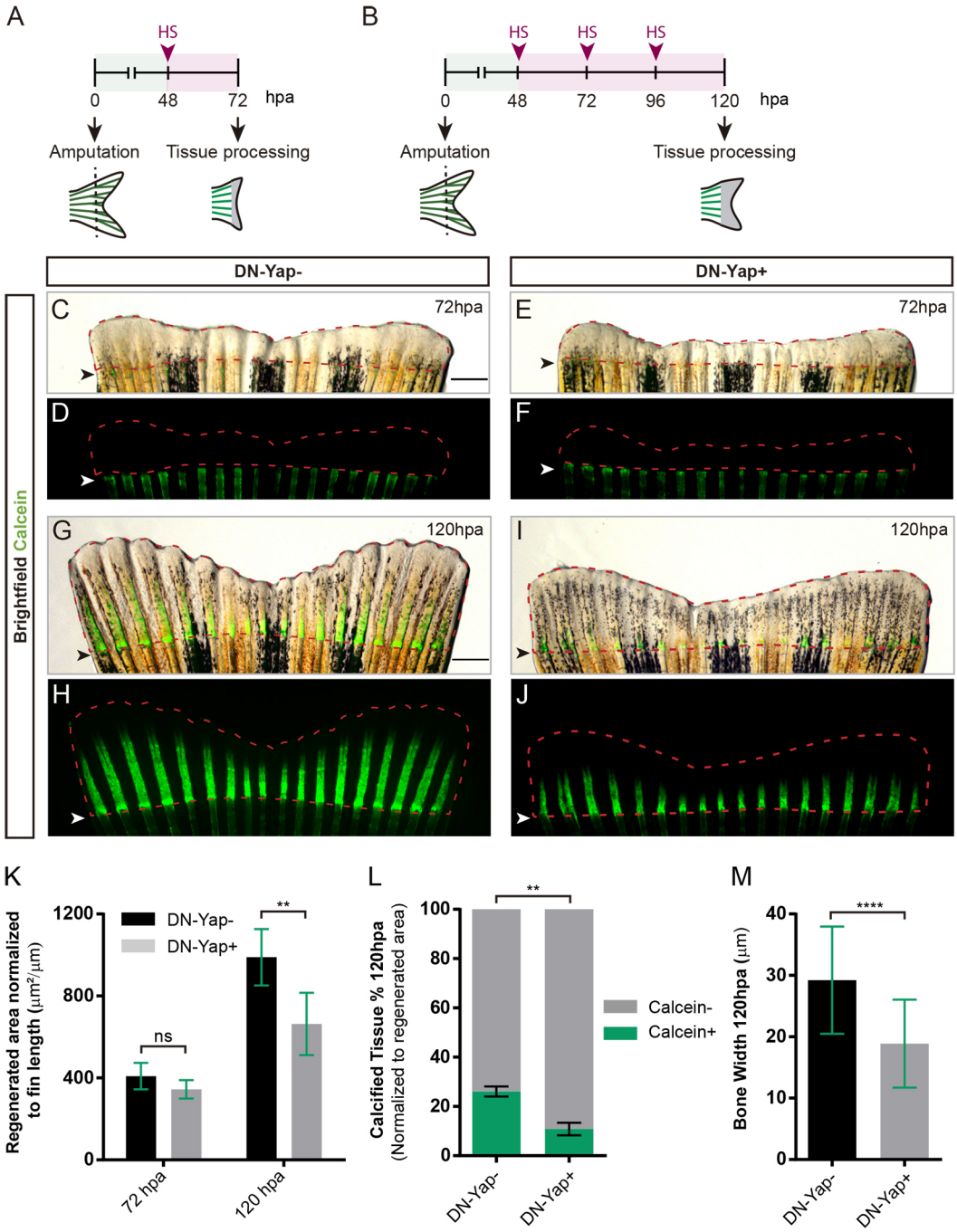

Fig. 1. Inhibition of Yap activity during regenerative outgrowth leads to bone formation defects. Experimental setup used for short (A) and prolonged (B) Yap inhibition protocols. HS, heat-shock. (C–J) Representative images of caudal fins stained for calcein (green) after short (C–F) and prolonged (G–J) Yap inhibition in DN-Yap− and DN-Yap+ fish. Dashed red lines outline the regenerated area. Arrowheads define the amputation plane. (K) Quantification of the regenerated area (n=4 fish in DN-Yap−; n=6 fish in DN-Yap+). (L) Percentage of calcified area (n=6 fish in DN-Yap− and in DN-Yap+). (M) Quantification of bony-ray width (n=54 bony-rays in DN-Yap−; n=36 bony-rays in DN-Yap+). Plot values represent means±s.d. **P<0.01; ****P<0.0001; ns, not significant (Mann–Whitney test). Scale bars: 0.5 mm.

at 72 hpa (Fig. 1A,C–F), which avoids temporal accumulation of Yap-mediated effects on cell proliferation and survival (Huang et al., 2005; Piccolo et al., 2014), allowing to investigate direct outcomes of Yap inhibition in the first stages of osteoblast differentiation. Second, we performed a prolonged Yap inhibition assay, consisting of daily heat-shocks from 48 to 96 hpa and fin analysis at 120 hpa (Fig. 1B,G–J), to determine the role of Yap in bony-ray formation. While the short inhibition did not have a significant impact on the total regenerated area (Fig. 1C–F,K), the prolonged inhibition resulted in a significant decrease in the regenerated area of DN-Yap+ fish (Fig. 1G–J,K). DN-Yap+ fish also presented a significant reduction in calcified bony-ray area (Fig. 1L) and reduced bony-ray width (Fig. 1M) at 120 hpa. These data show that a short Yap inhibition does not affect the overall fin regeneration, whereas prolonged Yap inhibition significantly reduces bone formation during regenerative outgrowth.

Yap regulates bone formation by inhibiting osteoprogenitor differentiation

Given the bone defects observed upon prolonged Yap inhibition, and since osteoblasts are fundamental for bone deposition, we hypothesized that the Hippo pathway might regulate osteoblast maturation. It has been described that, at the onset of outgrowth (48–72 hpa), osteoblasts initiate differentiation, exhibiting a proximo-distal hierarchical organization that can be monitored using different osteoblast markers (Brown et al., 2009) (Fig. 2A). Near the distal blastema (DB), self-renewing osteoprogenitors express *runx2* (Runx2$^+$; Stewart et al., 2014), a transcriptional regulator of mesenchymal cell commitment towards the osteoblast lineage (Ducy et al., 1997). The proximal blastema (PB) contains osteoblasts at the early stages of differentiation expressing both *runx2* and *osx* (Runx2$^+$ Osx$^+$; Stewart et al., 2014). The patterning zone (PZ), closer to the amputation plane, is populated by mature bone matrix-secreting osteoblasts expressing lower levels of *runx2* and high levels of *osx* and *bglap* (Brown et al., 2009). To investigate whether Yap is required for osteoblast differentiation, we monitored Yap subcellular localization, which reflects its activity status. Yap nuclear exclusion and cytoplasmic retention is often a read-out of inactivation, while its nuclear accumulation is associated with Yap-dependent transcriptional activity (Hansen et al., 2015; Zhao et al., 2007). We used a previously described Yap antibody (Rueda et al., 2019), which we further validated through western blotting of wild-type and *yap1* mutant samples (Fig. S1A), and by immunofluorescence in our Yap transgenic lines (Fig. S1B–G′).

Using reporter lines for *runx2* (Knopf et al., 2011) and *osx* (Singh et al., 2012), we characterized Yap subcellular localization at early stages of osteoblast differentiation (Fig. S1H–M″). Since Yap was mainly cytoplasmic in distal osteoprogenitors (DB, Fig. S1H,I–I″), in differentiating (PB, Fig. S1H,J–J″,K,L–L″) and in mature osteoblasts (PZ, Fig. S1K,M–M″), we conclude that Yap is likely inactive in all osteoblast populations during outgrowth. However, we observed that Yap was prominently nuclear in mesenchymal cells close to differentiating osteoblasts, mainly within the PZ and PB regions (Fig. S1H,J–J″,K,L–M″), suggesting Yap activation. To unravel the origin of the bone formation defects (Fig. 1G–J,L,M), we used the short Yap inhibition protocol, which has no effect on the overall regenerated area and allows us to uncouple the potential effects of Yap on cell proliferation and apoptosis, or on osteoblast differentiation. By quantifying the relative number of osteoblast subtypes and the total number of each osteoblast subtype per regenerated area after a short Yap inhibition (Fig. 2B–J), we noticed a significant increase in the number of osteoprogenitors (Runx2$^+$), and a reduction in the number of differentiating osteoblasts (Runx2$^+$ Osx$^+$) (Fig. 2H–J). Additionally, the osteoprogenitor domain, confined to distal regions in the control (Fig. 2B,D–D″), was expanded, with Runx2$^+$ cells found in more proximal locations in DN-Yap+ fish (Fig. 2E,F–F″). These results suggest that Yap inhibition does not disrupt the maintenance of the osteoprogenitor pool but instead prevents their differentiation into Runx2$^+$ Osx$^+$ osteoblasts. Supporting this, we observed fewer osteoprogenitors and an increase of differentiating osteoblasts in regenerating fins expressing a heat-shock-inducible constitutively active form of Yap *hsp70*:RFP-CAyap (hereafter referred as CA-Yap+) (Fig. S2A–C).

Furthermore, gene expression analyses (Fig. 2K) after the short Yap inhibition show that, while early progenitor markers such as *runx2* were unaltered, intermediate (immature) markers, such as *collagen 10a1* (*col10a1*), and mature markers like *osteonectin* (*osn*), were significantly downregulated in the DN-Yap+ regenerating fins. Similarly, prolonged Yap inhibition induced identical defects in osteoblast differentiation at the cellular (Fig. S2D–N) and transcriptional levels (Fig. S2O).

Considering the conserved roles of Yap in promoting cell proliferation and inhibiting apoptosis, we investigated whether the reduced number of differentiated osteoblasts after the short Yap inhibition was due to effects on apoptosis or proliferation. Analysis of cell death revealed that Yap inhibition induced an increase in apoptotic cells strictly in the external layers of the epidermis (Fig. S3A,B,E), indicating that the reduced number of differentiating osteoblasts is not due to increased apoptosis. Regarding proliferation, we observed an increase in the number of EdU-positive osteoblasts (Fig. S3C,D,F), which may explain the osteoprogenitor niche expansion; however, it does not account for the decrease in the differentiated osteoblasts subtype. Overall, these data suggest that Yap is critical for the engagement of the osteoblast differentiation programme. In addition, given that Yap is mainly cytoplasmic in osteoblasts, this regulation is potentially achieved via paracrine signalling.

Yap controls osteoblast differentiation by regulating Bmp signalling in a cell non-autonomous manner

Osteoprogenitor maintenance and differentiation are associated with antagonizing activities of Wnt and Bmp signalling, respectively. As distal osteoprogenitors proliferate, they become more proximal and activate autocrine Bmp signalling (Stewart et al., 2014). The newly formed basal epidermal layer (BEL) also influences osteoblast differentiation through Sonic hedgehog (Shh)-dependent *bmp2b* expression (Quint et al., 2002). To understand how Yap regulates osteoblast differentiation, we inhibited Yap function and analysed the expression of multiple components of key signalling pathways, such as Bmp (Smith et al., 2006), Wnt (Wehner et al., 2014), Shh (Laforest et al., 1998) and retinoic acid (RA) (Blum and Begemann, 2015). Upon a short Yap inhibition, we did not detect differences in the expression of *shh* or *bmp2b* transcripts (Fig. 3A). Furthermore, Yap is cytoplasmic (inactive) in the BEL cells (Fig. S4A–D′), indicating that it mediates osteoblast differentiation through an alternative mechanism.

Surprisingly, we observed a significant reduction of *dkk1a* (encoding a negative regulator of Wnt signalling; MacDonald et al., 2010) and *bmp2a* (encoding a ligand for Bmp signalling; Rosen, 2009) transcripts upon a short Yap inhibition (Fig. 3A), suggesting that Yap affects Wnt and Bmp signalling pathways during fin outgrowth. Notably, the same Yap-dependent transcriptional regulation was observed after prolonged Yap inhibition (Fig. S4E).

Journal of Cell Science (2019) 132, jcs231993. doi:10.1242/jcs.231993

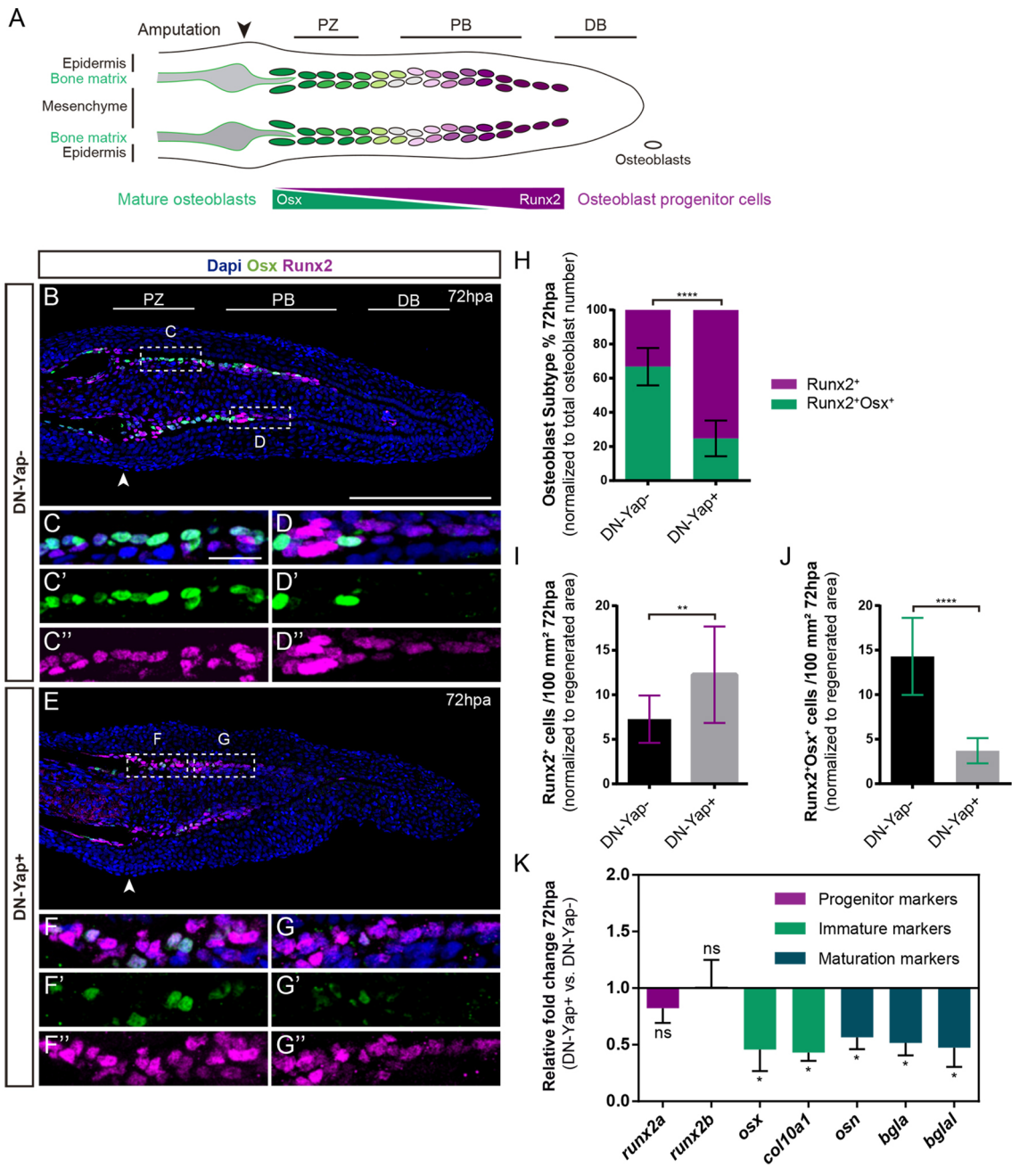

Fig. 2. Inhibition of Yap activity impairs osteoblast differentiation during regeneration. (A) Representation of a 72 hpa blastema, depicting osteoblast compartmentalization based on the expression of *osx* and *runx2* along the caudal fin proximo-distal axis. (B–G) Representative *z*-stack images of longitudinal cryosections from DN-Yap− (B–D″) and DN-Yap+ (E–G″) caudal fins immunostained for Runx2 (magenta), Osx (green) and DAPI (blue). Regions bounded by dashed boxes are magnifications of the PZ (C,F) and PB regions (D,G). Arrowheads define the amputation plane. (H–J) Percentage of osteoblast subtypes (H) and quantification of Runx2$^+$ osteoblasts (I) and Runx2$^+$ Osx$^+$ (J) in DN-Yap− and DN-Yap+ fins (*n*=15 cryosections in DN-Yap−; *n*=19 cryosections in DN-Yap+). (K) Relative gene expression of progenitor, immature and late osteoblast markers (*n*=4 biological replicates). Plot values represent means±s.d., **P*<0.05; ***P*<0.01; *****P*<0.0001; ns, not significant (Mann–Whitney test). Scale bars: 200 µm (B), 20 µm (C).

Since Yap interacts with both signalling pathways in other systems (Attisano and Wrana, 2013), we investigated its subcellular localization in relation to activated Bmp and Wnt signalling during osteoblast differentiation. We first measured the percentage of mesenchymal cells with active (mainly nuclear) Yap and phosphorylated (active) Smad1, 5 and 8 (hereafter referred to as pSmad1/5/8), the Bmp signalling effector (Wu et al., 2016; Fig. 3B–E). Yap was predominantly nuclear in 55% of the mesenchymal cells within the PZ and PB, whereas only 25% presented nuclear pSmad1/5/8 (Fig. 3B–B″,C–C″,D–D″,E). In the DB region, only a minority of cells presented nuclear Yap and/or pSmad1/5/8 (Fig. 3B,B‴,C,C‴,D,D‴,E). In accordance with previous reports (Stewart et al., 2014), Bmp signalling was mainly active in differentiating osteoblasts that populate the PZ and PB compartments (Fig. 3B–B″,D′–D″,F), while in the DB region pSmad1/5/8-positive osteoblasts are less evident (Fig. 3B,B‴,D,D‴,F). These results show that, although Yap and Bmp signalling are active in different cell types, such as mesenchyme and osteoblasts,

Journal of Cell Science (2019) 132, jcs231993. doi:10.1242/jcs.231993

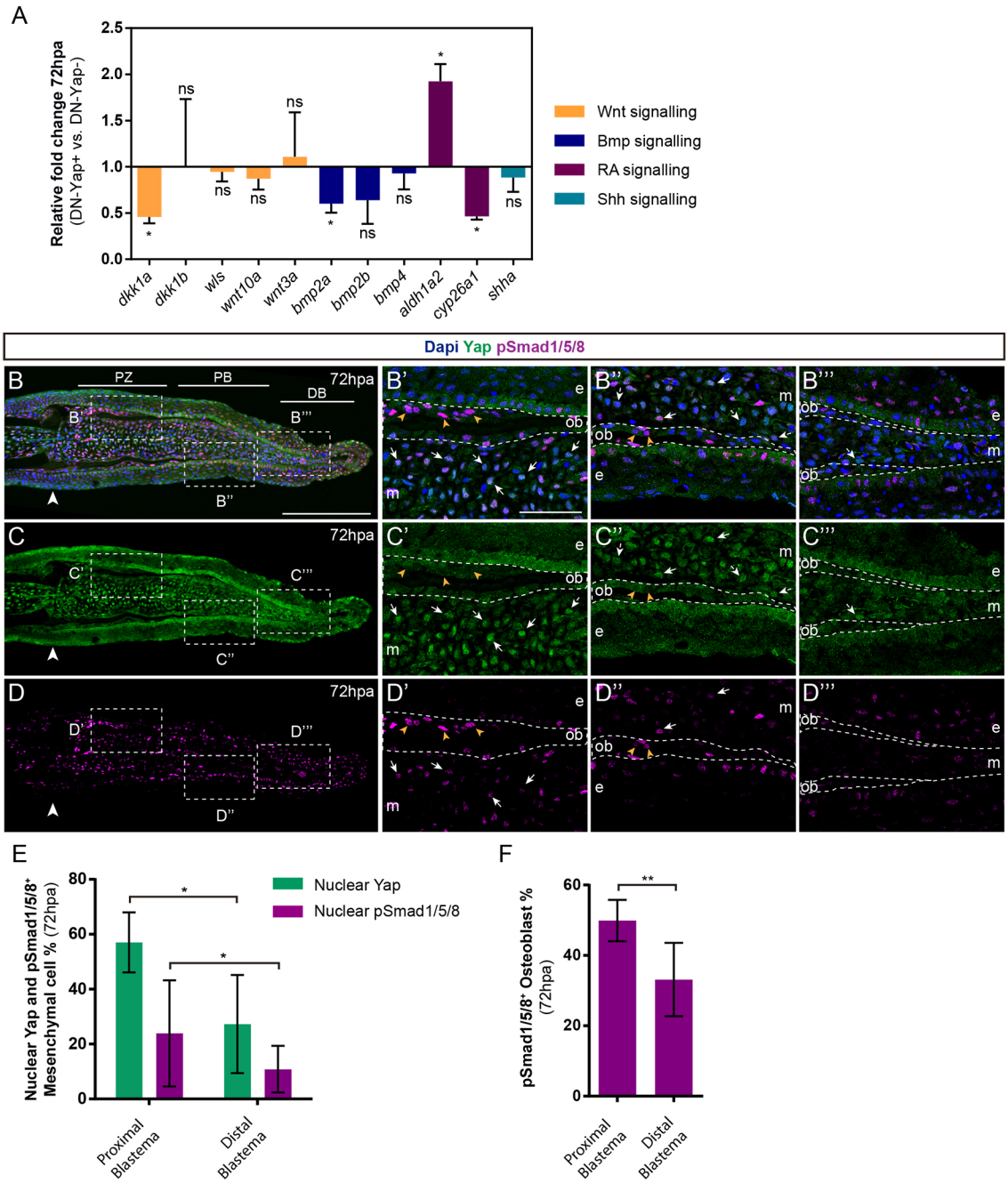

Fig. 3. Yap and Bmp signalling share similar proximo-distal activity profiles in distinct blastema populations. (A) Relative gene expression of multiple signalling pathway components required for bone formation after a short Yap inhibition (n=4 biological replicates). (B–D) Representative z-stack image of a longitudinal fin cryosection immunostained for Yap (green), pSmad1/5/8 (magenta) and DAPI (blue). Dashed boxes are magnifications of the PZ (B′,C′,D′), PB (B″,C″,D″) and DB (B‴,C‴,D‴) regions. White arrows point to mesenchymal cells with nuclear Yap and pSmad1/5/8, dashed arrows to nuclear Yap and pSmad1/5/8-negative cells and orange arrowheads to osteoblasts with nuclear pSmad1/5/8 and cytoplasmic Yap. Dashed white lines delineate the different tissue compartments. Large white arrowheads define the amputation plane. m, mesenchyme; ob, osteoblasts; e, epidermis. (E,F) Percentage of nuclear Yap and pSmad1/5/8-positive mesenchymal cells (E) and pSmad1/5/8-positive osteoblasts (F) in PB and DB regions (n=9 cryosections). Plot values represent means±s.d. *P<0.05; **P<0.01; ns, not significant (Mann–Whitney test). Scale bars: 200 µm, (B) 50 µm (B′).

respectively, they share a proximo-distal gradient of activation: more inactive distally and progressively more active towards proximal regions. Thus, we speculate that Yap may induce *bmp2a* expression in mesenchymal cells within the PB, which activates Bmp signalling in adjacent osteoblasts, promoting differentiation. To test this hypothesis, we evaluated whether short Yap inhibition perturbs Bmp signalling activation in osteoblasts (Fig. 4A–G). In contrast to controls (Fig. 4A–C′,G,H), a short Yap inhibition led to a clear reduction in the number of pSmad1/5/8-positive cells in osteoblast (labelled with Zns5, a pan-osteoblast marker) and mesenchymal populations (Fig. 4D–F′,G,H), indicative of Yap requirement for Bmp signalling activation. These results suggest a new role for Yap in mesenchymal cells and their contribution as a source of Bmp ligands that influence the adjacent tissues, particularly the osteoblasts.

Moreover, Bmp signalling promotes Dkk1b secretion, restricting Wnt signalling to the DB compartment for progenitor maintenance

Journal of Cell Science (2019) 132, jcs231993. doi:10.1242/jcs.231993

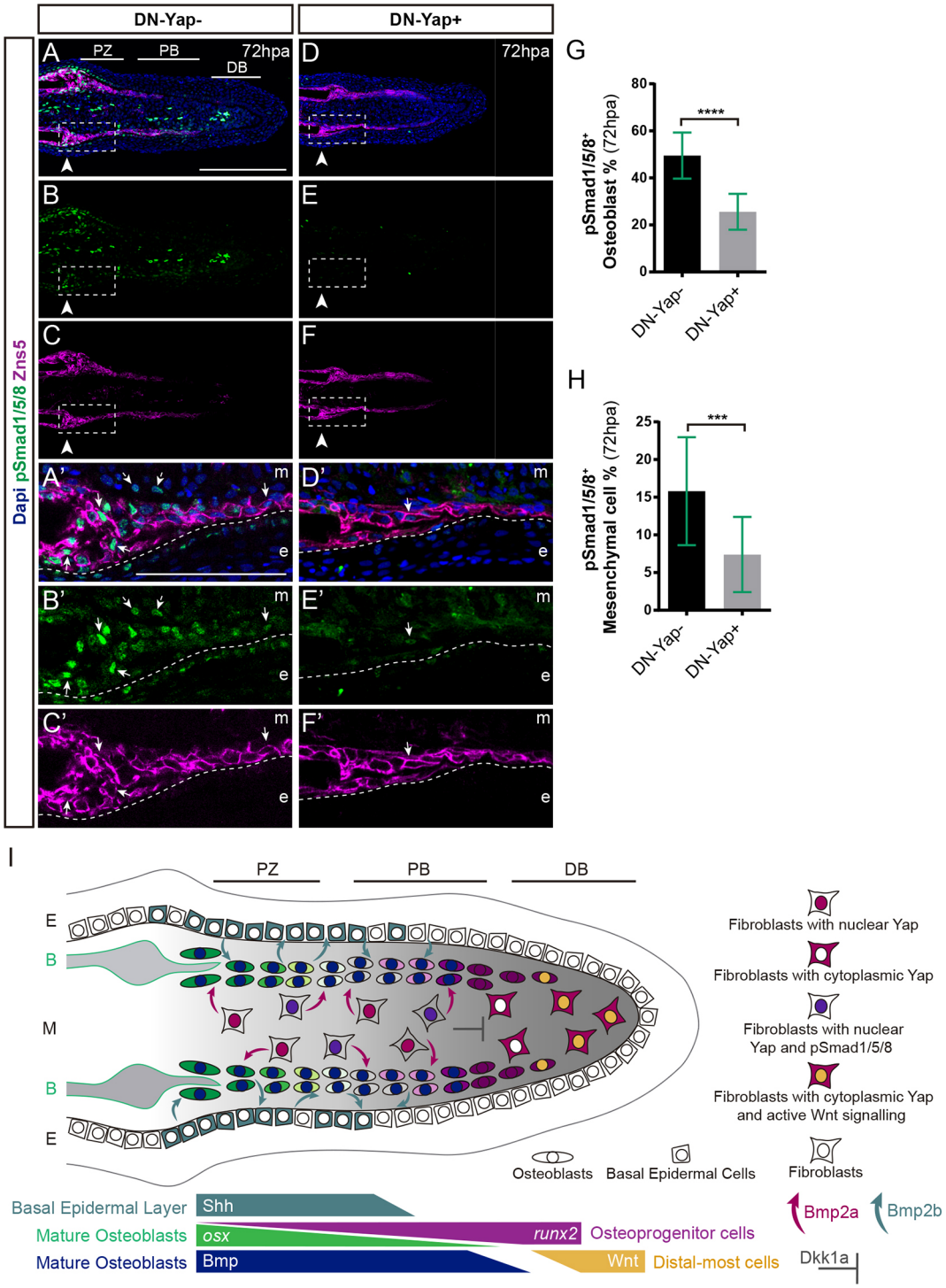

Fig. 4. Manipulation of Yap activity inhibits Bmp signalling during regeneration. (A–F′) Representative z-stack images of longitudinal cryosections of DN-Yap– (A-C′) and DN-Yap+ (D-F′) caudal fins immunostained for Zns5 (magenta), pSmad1/5/8 (green) and DAPI (blue). Dashed boxes show magnified areas from the PZ regions (A′–F′). Arrows and dashed arrows point to osteoblasts (Zns5^{+}) and mesenchymal cells with nuclear pSmad1/5/8, respectively. White arrowheads define the amputation plane and white dashed lines the interface between osteoblasts and epidermis. m, mesenchyme; e, epidermis; b, bone. (G) Quantification of pSmad1/5/8-positive osteoblasts (n=21 cryosections in DN-Yap–; n=19 cryosections in DN-Yap+). (H) Percentage of pSmad1/5/8-positive mesenchymal fibroblasts (n=11 cryosections in DN-Yap–; n=12 cryosections in DN-Yap+). (I) Our proposed model on osteoblast differentiation in caudal fin bone regeneration highlighting the main signalling players. Plot values represent means±s.d. ***P<0.001, ****P<0.0001 (Mann–Whitney test). Scale bars: 200 µm (A), 50 µm (A′).

(Stewart et al., 2014). By using a reporter line for Wnt signalling activity (Moro et al., 2012), we observed that while Wnt is mainly active in the DB compartment, Yap is mostly cytoplasmic, suggesting antagonist activities (Fig. S4F–I″,J). Furthermore, the downregulation of *dkk1a* (Fig. 3A; Fig. S4A) and increase of the osteoprogenitor pool upon Yap inhibition might imply that Yap and Bmp signalling act synergistically during fin regeneration restricting Wnt signalling activity to the distal-most region of the fin.

Overall, our data indicate a new mechanism by which Yap establishes spatial relationships between the mesenchyme and

osteoblasts, thereby dictating key cell fate decisions during fin regeneration. We show that the Hippo-Yap pathway is fundamental to direct proper osteoblast differentiation by acting in a cell non-autonomous manner (Fig. 4I). On one hand, together with Bmp signalling, Yap may inhibit Wnt signalling expansion to the PB by regulating the expression of *dkk1a*, consequently restricting osteoprogenitors to the DB. On the other hand, and more importantly, Yap promotes the production of Bmp2a in mesenchymal cells in proximal regions, which is crucial for Bmp signalling activation in adjacent osteoblasts and hence osteoblast differentiation (Fig. 4I). These findings provide a deeper understanding of the mechanisms regulating bone regeneration and clarify the role of the Hippo-Yap signalling pathway during osteoblast lineage specification.

MATERIALS AND METHODS

Ethics statement

All the people involved in animal handling and experimentation were properly trained and accredited by FELASA. All experimental procedures were approved by the Animal User and Ethical Committees at Centro de Estudos de Doenças Crónicas (CEDOC) and accredited by the Portuguese National Authority for Animal Health (DGAV) according to the directives from the European Directive (2010/63/UE) and Portuguese legislation (Decreto-Lei 113/2013) for animal experimentation and welfare.

Zebrafish lines and mutants

Wild-type AB, *Tg(osterix:mCherryNTRo)*^{pd46} (Singh et al., 2012), *Tg(Has.RUNX2-Mmu.Fos:EGFP)*^{zf259} (Knopf et al., 2011), *Tg(7xTCF-Xla.Siam:GFP)*^{ia4} (Moro et al., 2012), *Tg(hsp70l:RFP-dnyap1)*^{zf621} and *Tg(hsp70l:RFP-cayap1)*^{zf622} (Mateus et al., 2015) zebrafish lines were maintained in a circulating system with 14 h day and 10 h night cycle periods at 28°C. All regeneration experiments were performed in 4–18-month-old adult fish (Westerfield, 2000) and all transgenic animals were used as heterozygotes. Homozygous *yap1*^{bns19} CRISPR mutants (Kimelman et al., 2017) and wild-type AB strain embryos used for antibody validation by western blotting were maintained at 28°C in E3 medium until 3 days post-fertilization (dpf).

Caudal fin amputation and heat-shock experiments

Caudal fin amputations were performed in fish anaesthetized with buffered 160 mg/ml MS-222 (Sigma, E10521) using a sterile scalpel. Regeneration was allowed to proceed until defined time-points in an incubator at 33°C±1°C with light cycle, except for heat-shock experiments, which were performed at 28°C, and the water was renewed daily. Amputations were made 1 or 2 segments below the most proximal ray bifurcation, removing approximately one half of the fin. Regenerated fins were collected from anaesthetized fish, as previously described (Poss et al., 2000). For heat-shock experiments, Tg(*hsp70l:*RFP-*dnyap1*), Tg(*hsp70l:*RFP-*cayap1*) and corresponding negative siblings were maintained and heat-shocked as previously described (Mateus et al., 2015). For Yap inhibition assays, animals were left to regenerate normally during the blastema formation phase (0–48 hpa), and heat-shocked afterwards. For short period manipulations (short Yap inhibition protocol), animals were heat-shocked once at 48 hpa and fins collected 24 h after. For long period manipulations (prolonged Yap inhibition protocol), animals were heat-shocked at 48, 72 and 96 hpa, and fins were collected at 120 hpa. Fins were then processed for cryosectioning or pooled for RNA extraction.

Total RNA isolation and quantitative real-time PCR

For gene expression analysis, caudal fin regenerates were collected, including one bony-ray segment proximal to the amputation plane. Pools from four caudal fins were used per biological replicate, and four biological replicates were used per time-point. Briefly, samples were homogenized in Trizol reagent (Invitrogen, 15596026) for cell disruption and RNA extraction. Chloroform was added, and the homogenate allowed to separate into a clear upper aqueous layer. RNA was precipitated and purified from the aqueous phase by adding an equal amount of 100% ethanol and loading the mixture into RNeasy Micro Spin columns (Qiagen, 74004). The remaining procedure was done following the RNeasy Micro kit (Qiagen, 74004) manufacturer's protocol. cDNA was synthesized from 1 µg total RNA for each sample using the Transcriptor high-fidelity cdna synthesis kit (Roche, 05081963001), with a mixture of oligo(dT) and random primers. All quantitative real-time PCR (qPCR) primers are listed in Table S1. qPCR was performed using a FastStart Essential DNA Green master mix (Roche, 4385617) and a Roche LightCycler 480. Cycle conditions were: 15 min pre-incubation at 95°C and three-step amplification cycles (50×), each cycle for 30 s at 95°C, 15 s at 65°C or 68°C (depending on primer melting temperature) and for 30 s at 72°C.

EdU incorporation assay

For ethynyl-2′-deoxyuridine (EdU, Thermo Scientific: C10337) labelling, animals were subjected to caudal fin amputation, as described above, and allowed to regenerate until the desired time-points. Animals were anesthetized 3 h prior to caudal fin collection, and administered, via intraperitoneal injection, with 20 µl of 10 mM EdU solution (2.5 mg/ml stock solution in DMSO diluted in 1× PBS). Injections were performed with an U-100 G 0.3 ml insulin syringe and a 30 G needle (BD Micro-fine) inserted close to the pelvic girdle. Upon collection, caudal fins were fixed in 4% paraformaldehyde and processed for cryosectioning.

Calcein staining, immunofluorescence and image acquisition

Calcein (Sigma-Aldrich, C0875-56) staining, used to label the regenerated bony-rays, was performed as previously described (Du et al., 2001). Fins were imaged using a Zeiss Lumar V-12 fluorescence stereoscope equipped with a Zeiss digital camera using a 0.8× air objective and the Zen 2 PRO blue software.

Caudal fin fixation, preservation and embedding was performed as previously described (Mateus et al., 2015). For EdU labelling, caudal fins were fixed and directly incubated in 30% sucrose solution. Longitudinal caudal fin sections were cut with 12 µm-thickness using a Microm cryostat (Cryostat Leica CM3050 S) and stored at −20°C until further use. For immunofluorescence on cryosections, sections were thawed for 15 min at room temperature, washed twice in 1× PBS at 37°C for 10 min, followed by a 0.1 M glycine (Sigma-Aldrich, in 1× PBS) incubation for 10 min. Sections were then permeabilized in acetone for 7 min at −20°C and incubated for 20 min in 0.2% PBST (1× PBS with 0.2% Triton X-100). At this point, cryosections used for EdU staining were incubated with the labelling solution according to the manufacturer's protocol (Thermo Fisher Scientific, C10337). For the TUNEL labelling assay, cryosections were permeabilized in a sodium citrate solution (0.1% sodium citrate and 0.1% Triton X-100 in 1× PBS) and labelled according to the manufacturer's protocol (Roche, 11684795910).

For anti-Runx2 and anti-Osx antibody staining, an antigen retrieval step was performed, which consisted of a 15-min incubation at 95°C with sodium citrate buffer (10 mM Tri-sodium citrate with 0.05% Tween 20, pH 6). For anti-pSmad1/5/8 and anti-Zns5 staining, slides were incubated in a blocking solution of 10% non-fat dry milk in PBST, containing 650 mM NaCl, and subsequently washed with PBST, containing 650 mM NaCl as previously described (Stewart et al., 2014). For anti-Yap staining, slides were washed in PBDX (1% BSA, 1% DMSO, 0.2% Triton-100, 50% PBS 1× in Milli-Q water) and blocked in PBDX containing 1.5% goat serum as has been previously described (Mateus et al., 2015). Incubation with anti-YAP was performed overnight at room temperature. Antibody details are provided in Table S2.

Images were acquired in a Zeiss LSM 710 and Zeiss LSM 880 confocal microscope using the software ZEN 2010B SP1 and processed and analysed using the Fiji-ImageJ software (Schindelin et al., 2012). Caudal fin section *z*-stacks were acquired using a 40× water or a 40×1.2 NA multi-immersion objective with 0.6× or 1× zoom and a step size of 1 µm. For image processing, composite maximum intensity *z*-stack projections were made, except when noted. Concatenation of several images along the proximal-distal axis of the same longitudinal section was performed using the Fiji plugin 3D Pairwise Stitching.

Western blotting

Lysates of MCF-7 human breast adenocarcinoma cell line (ATCC, HTB-22) were obtained by freeze-thaw (5 cycles, 5 min in dry ice), 20 min incubation at 37°C and subsequent centrifugation (2000 ***g*** for 10 min). 3 dpf wild-type and *yap1*^{bns19} zebrafish mutant larvae were lysed with Tris buffer (100 mM Tris-HCl pH 9.5, 1% SDS), sonicated and centrifuged (16,000 ***g*** for 10 min at 4°C). Protein concentration from supernatants was determined using Pierce BCA protein assay kit (Thermo Fisher Scientific). Laemmli buffer was added to 5 µg of protein and samples were heated at 95°C for 5 min. Total protein was resolved on a 10% SDS gel and transferred to a nitrocellulose membrane during 75 min at 100 V. The membranes were blocked with Tris-buffered saline (TBS) with 0.1% Tween 20 (TBST) containing 5% skimmed milk, followed by incubation with primary mouse anti-YAP (63.7) (1:500, Santa Cruz Biotechnology, sc101199) and mouse anti-α-tubulin (1:1000, Cell Signaling, 3873S) antibodies in TBST containing 1% skimmed milk. Membranes were incubated with HRP-conjugated secondary goat anti-mouse-IgG (1:5000, Bio-Rad: 1706516) antibodies. Images were acquired using ChemiDoc Touch System (BioRad).

Quantifications and statistical analysis

For qPCR analysis, all samples were analysed in four biological pools. For each biological pool, qPCR was performed for each target gene in three technical replicates. Gene expression values were normalized using the *elongation factor 1α* (*ef1α*, NM_131263) housekeeping gene and relative expression was calculated using the 2[−ΔΔC(T)] method (Livak and Schmittgen, 2001).

Measurements of the total regenerated area at 72 hpa and at 120 hpa were performed using images of whole caudal fins. The regenerated fin area was delineated from the amputation plane to the distal end of the regenerated area using the Area tool in Fiji. The regenerated area was then normalized to the corresponding total caudal fin width to avoid discrepancies related to the animal size, resulting in one measurement per animal. Four to six animals were used per condition.

The percentage of bony-ray formation at 120 hpa was defined by the area stained by calcein in relation to the total fin regenerated area. Briefly, the area of fluorescence intensity for each image was determined by empirically establishing a threshold to separate the signal fluorescence intensity from the background. The average fluorescence area was then normalized to the total tissue regenerate area as described above, resulting in one measurement per animal. Six animals were used per condition.

Determination of bony-ray width at 120 hpa in calcein staining experiments, was performed automatically by thresholding the fluorescence signal, which was determined using the Otsu algorithm in Fiji. Subsequently, the width at the base of each formed bony-ray was measured using the line tool on Fiji. Individual bony-ray widths from three different animals are plotted in a graph (56 bony-rays from Sibling controls and 36 bony-rays from DN-Yap^{+} transgenics).

The Yap subcellular localization and the number of pSmad1/5/8-positive cells in proximal and distal blastema regions of caudal fin cryosections were quantified using a custom-made Fiji macro (available upon request). The macro automatically finds the nuclei in individual *z*-stack slices, searches for the signal surrounding the nuclei and compares the nuclear fluorescence intensity with the surrounding cytoplasmic fluorescence intensity. The nuclei images were pre-processed using a median filter with a kernel size of 2 pixels for noise removal. Local thresholding was performed using the Phansalkar method with a kernel size of 15 pixels. The resultant binary image was morphologically closed to fill holes. Finally, nuclei masks were created using the 'Analyse particles' plugin. The signal surrounding the nuclei was found by enlarging each nuclear mask by 3 pixels and removing the correspondent nuclear region. The average signal intensity for both regions was obtained and a ratio was calculated (nuclear/cytoplasmic). A positive (nuclear) Yap signal was considered when this ratio was above 1.2. For quantification of the number of cells presenting nuclear pSmad1/5/8, the same nuclei mask was used. Positive (nuclear) pSmad1/5/8 signal was identified automatically using thresholding. Since the signal to noise ratio is high, the threshold value was selected manually using an average value between the background and the positive nuclei signals. Nine cryosections from three different animals are plotted.

The total number of osteoblast subtypes (Runx2^{+} or Runx2^{+}Osx^{+}) was quantified by analysing the number of cells in relation to the total regenerated area (per 100 µm^{2}), determined using the Area tool on Fiji. The percentage of osteoblast subsets (Runx2^{+} or Runx2^{+} Osx^{+}) and pSmad1/5/8-positive cells in longitudinal cryosections was quantified by analysing the number of cells in the regenerated area in relation to the total number of osteoblast (Runx2^{+} and Runx2^{+} Osx^{+} or Zns5-positive cells). Quantifications were performed using the Cell-counter plugin on Fiji on individual cryosections representing at least three different blastemas per animal and three or four animals per condition. For osteoblast subtype quantification after the short Yap inhibition protocol, 15 cryosections from DN-Yap− and 19 cryosections from DN-Yap+ were used. For the prolonged inhibition protocol, 15 cryosections from both DN-Yap− and DN-Yap+ were analysed. In the CA-Yap manipulation protocol, 11 cryosections from CA-Yap− and 15 cryosections from CA-Yap+ were used. For quantification of pSmad1/5/8-positive cells within the total osteoblast population (Zns5^{+} population), we analysed 19 cryosections in DN-Yap+ and 21 cryosections in sibling controls. For quantification of pSmad1/5/8-positive cells within the mesenchymal population, 11 cryosections in DN-Yap− and 12 cryosections in DN-Yap+ were analysed.

The total number of TUNEL- and EdU-positive cells was quantified by analysing the number of labelled cells in each caudal fin compartment (epidermis, mesenchyme and Zns5-positive osteoblasts) in relation to the corresponding compartment regenerated area (per 100 µm^{2}), as determined using the Area tool on Fiji. Quantifications were undertaken using the Cell-counter plugin on Fiji in individual cryosections representing at least three different blastemas per animal and three animals used for TUNEL labelling and four animals for EdU labelling per condition. For TUNEL, 19 cryosections from DN-Yap− and 18 cryosections from DN-Yap+ were quantified. For EdU labelling, 25 cryosections from DN-Yap− and n=21 cryosections from DN-Yap+ were analysed.

Statistical significance between controls and manipulated animals was determined using an unpaired, non-parametric Mann–Whitney *U*-test in the Prism Graphpad software. Means and standard deviations (s.d.) are displayed in the graphs. P<0.05 was considered statistically significant.

Acknowledgements

We are grateful to Lara Carvalho and Inês Cristo for reading the manuscript, Duarte Mesquita for discussion, and Telmo Pereira, Ana Farinho and Diana Saraiva for technical assistance. We thank the CEDOC Fish, Histology and Microscopy facilities for support and Kenneth Poss, Gilbert Weidinger, Didier Stainier and Jason Lai for zebrafish transgenic and mutant line sharing. A.B.-B. thanks Didier Stainier for salary support during the preparation of this manuscript.

Competing interests

The authors declare no competing or financial interests.

Author contributions

Conceptualization: A.S.B., A.B.-B., R.M.; Methodology: A.S.B., A.B.-B., R.L., J.B., A.R.S.; Validation: A.S.B.; Formal analysis: A.S.B.; Investigation: A.S.B., R.L., J.B., A.R.S.; Writing - original draft: A.S.B.; Writing - review & editing: A.S.B., A.B.-B., R.L., J.B., A.J.; Visualization: A.S.B., A.B.-B.; Supervision: A.B.-B., A.J.; Project administration: A.J.; Funding acquisition: A.J.

Funding

This work was funded by Fundação para a Ciência e a Tecnologia (FCT; PTDC/BIM-MED/0659/2014; SFRH/BD/51990/2012 to A.S.B.; SFRH/BD/131929/2017 to J.B.; PD/BD/106052/2015 to A.R.S.). R.L. was supported by the FCT in the context of a program contract (D.L. no. 57/2016). Zebrafish maintenance was supported by Congento LISBOA-01-0145-FEDER-022170, co-financed by FCT (Portugal) and Lisboa2020, under the PORTUGAL2020 agreement (European Regional Development Fund).

Supplementary information

Supplementary information available online at
http://jcs.biologists.org/lookup/doi/10.1242/jcs.231993.supplemental

References

Ando, K., Shibata, E., Hans, S., Brand, M. and Kawakami, A. (2017). Osteoblast production by reserved progenitor cells in zebrafish bone regeneration and maintenance. *Dev. Cell* **43**, 643-650.e3. doi:10.1016/j.devcel.2017.10.015

Antos, C. L., Knopf, F. and Brand, M. (2016). Regeneration of Organs and Appendages in Zebrafish: A Window into Underlying Control Mechanisms. eLS, John Wiley & Sons, Ltd. doi:10.1002/9780470015902.a0022101.pub2

Attisano, L. and Wrana, J. L. (2013). Signal integration in TGF-β, WNT, and Hippo pathways. *F1000 Prime Rep.* **5**, 17. doi:10.12703/P5-17

Blum, N. and Begemann, G. (2015). Osteoblast de- and redifferentiation are controlled by a dynamic response to retinoic acid during zebrafish fin regeneration. *Development* **142**, 2894-2903. doi:10.1242/dev.120204

Brown, A. M., Fisher, S. and Iovine, M. K. (2009). Osteoblast maturation occurs in overlapping proximal-distal compartments during fin regeneration in zebrafish. *Dev. Dyn.* **238**, 2922-2928. doi:10.1002/dvdy.22114

Corrado, A., Sanpaolo, E. R., Di Bello, S. and Cantatore, F. P. (2017). Osteoblast as a target of anti-osteoporotic treatment. *Postgrad. Med.* **129**, 858-865. doi:10.1080/00325481.2017.1362312

Dimitriou, R., Jones, E., McGonagle, D. and Giannoudis, P. V. (2011). Bone regeneration: current concepts and future directions. *BMC Med.* **9**, 66. doi:10.1186/1741-7015-9-66

Du, S. J., Frenkel, V., Kindschi, G. and Zohar, Y. (2001). Visualizing normal and defective bone development in zebrafish embryos using the fluorescent chromophore calcein. *Dev. Biol.* **238**, 239-246. doi:10.1006/dbio.2001.0390

Ducy, P., Zhang, R., Geoffroy, V., Ridall, A. L. and Karsenty, G. (1997). Osf2/Cbfa1: A transcriptional activator of osteoblast differentiation. *Cell* **89**, 747-754. doi:10.1016/S0092-8674(00)80257-3

El Bialy, I., Jiskoot, W. and Reza Nejadnik, M. (2017). Formulation, delivery and stability of bone morphogenetic proteins for effective bone regeneration. *Pharm. Res.* **34**, 1152-1170. doi:10.1007/s11095-017-2147-x

Halder, G., Dupont, S. and Piccolo, S. (2012). Transduction of mechanical and cytoskeletal cues by YAP and TAZ. *Nat. Rev. Mol. Cell Biol.* **13**, 591-600. doi:10.1038/nrm3416

Hansen, C. G., Moroishi, T. and Guan, K.-L. (2015). YAP and TAZ: a nexus for Hippo signaling and beyond. *Trends Cell Biol.* **25**, 499-513. doi:10.1016/j.tcb.2015.05.002

Huang, J., Wu, S., Barrera, J., Matthews, K. and Pan, D. (2005). The Hippo signaling pathway coordinately regulates cell proliferation and apoptosis by inactivating Yorkie, the Drosophila homolog of YAP. *Cell* **122**, 421-434. doi:10.1016/j.cell.2005.06.007

Irvine, K. D. (2012). Integration of intercellular signaling through the Hippo pathway. *Semin. Cell Dev. Biol.* **23**, 812-817. doi:10.1016/j.semcdb.2012.04.006

Kawakami, A. (2010). Stem cell system in tissue regeneration in fish. *Dev. Growth Differ.* **52**, 77-87. doi:10.1111/j.1440-169X.2009.01138.x

Kegelman, C. D., Mason, D. E., Dawahare, J. H., Horan, D. J., Vigil, G. D., Howard, S. S., Robling, A. G., Bellido, T. M. and Boerckel, J. D. (2018). Skeletal cell YAP and TAZ combinatorially promote bone development. *FASEB J.* **32**, 2706-2721. doi:10.1096/fj.201700872R

Kimelman, D., Smith, N. L., Lai, J. K. H. and Stainier, D. Y. R. (2017). Regulation of posterior body and epidermal morphogenesis in zebrafish by localized Yap1 and Wwtr1. *eLife* **6**, e31065. doi:10.7554/eLife.31065

Knopf, F., Hammond, C., Chekuru, A., Kurth, T., Hans, S., Weber, C. W., Mahatma, G., Fisher, S., Brand, M., Schulte-Merker, S. et al. (2011). Bone regenerates via dedifferentiation of osteoblasts in the zebrafish fin. *Dev. Cell* **20**, 713-724. doi:10.1016/j.devcel.2011.04.014

Laforest, L., Brown, C. W., Poleo, G., Géraudie, J., Tada, M., Ekker, M. and Akimenko, M.-A. (1998). Involvement of the sonic hedgehog, patched 1 and bmp2 genes in patterning of the zebrafish dermal fin rays. *Development* **125**, 4175-4184.

Livak, K. J. and Schmittgen, T. D. (2001). Analysis of relative gene expression data using real-time quantitative PCR and the 2-ΔΔCT method. *Methods* **25**, 402-408. doi:10.1006/meth.2001.1262

Long, F. (2012). Building strong bones: molecular regulation of the osteoblast lineage. *Nat. Rev. Mol. Cell Biol.* **13**, 27-38. doi:10.1038/nrm3254

MacDonald, B. T., Tamai, K. and He, X. (2010). Wnt/β-catenin signaling: components, mechanisms, and diseases. *Dev. Cell* **17**, 9-26. doi:10.1016/j.devcel.2009.06.016

Marí-Beffa, M. and Murciano, C. (2010). Dermoskeleton morphogenesis in zebrafish fins. *Dev. Dyn.* **239**, 2779-2794. doi:10.1002/dvdy.22444

Mateus, R., Lourenco, R., Fang, Y., Brito, G., Farinho, A., Valerio, F. and Jacinto, A. (2015). Control of tissue growth by Yap relies on cell density and F-actin in zebrafish fin regeneration. *Development* **142**, 2752-2763. doi:10.1242/dev.119701

Misra, J. R. and Irvine, K. D. (2018). The Hippo signaling network and its biological functions. *Annu. Rev. Genet.* **52**, 65-87. doi:10.1146/annurev-genet-120417-031621

Moro, E., Ozhan-Kizil, G., Mongera, A., Beis, D., Wierzbicki, C., Young, R. M., Bournele, D., Domenichini, A., Valdivia, L. E., Lum, L. et al. (2012). In vivo Wnt signaling tracing through a transgenic biosensor fish reveals novel activity domains. *Dev. Biol.* **366**, 327-340. doi:10.1016/j.ydbio.2012.03.023

Moya, I. M. and Halder, G. (2019). Hippo–YAP/TAZ signalling in organ regeneration and regenerative medicine. *Nat. Rev. Mol. Cell Biol.* **20**, 211-226. doi:10.1038/s41580-018-0086-y

Nakashima, K., Zhou, X., Kunkel, G., Zhang, Z., Deng, J. M., Behringer, R. R. and de Crombrugghe, B. (2002). The novel zinc finger-containing transcription factor Osterix is required for osteoblast differentiation and bone formation. *Cell* **108**, 17-29. doi:10.1016/S0092-8674(01)00622-5

Pan, J.-X., Xiong, L., Zhao, K., Zeng, P., Wang, B., Tang, F.-L., Sun, D., Guo, H.-H., Yang, X., Cui, S. et al. (2018). YAP promotes osteogenesis and suppresses adipogenic differentiation by regulating β-catenin signaling. *Bone Res.* **6**, 18. doi:10.1038/s41413-018-0018-7

Pfefferli, C. and Jaźwińska, A. (2015). The art of fin regeneration in zebrafish. *Regeneration* **2**, 72-83. doi:10.1002/reg2.33

Piccolo, S., Dupont, S. and Cordenonsi, M. (2014). The Biology of YAP/TAZ: Hippo signaling and beyond. *Physiol. Rev.* **94**, 1287-1312. doi:10.1152/physrev.00005.2014

Poss, K. D., Shen, J., Nechiporuk, A., McMahon, G., Thisse, B., Thisse, C. and Keating, M. T. (2000). Roles for Fgf signaling during zebrafish fin regeneration. *Dev. Biol.* **222**, 347-358. doi:10.1006/dbio.2000.9722

Poss, K. D., Keating, M. T. and Nechiporuk, A. (2003). Tales of regeneration in zebrafish. *Dev. Dyn.* **226**, 202-210. doi:10.1002/dvdy.10220

Quint, E., Smith, A., Avaron, F., Laforest, L., Miles, J., Gaffield, W. and Akimenko, M.-A. (2002). Bone patterning is altered in the regenerating zebrafish caudal fin after ectopic expression of sonic hedgehog and bmp2b or exposure to cyclopamine. *Proc. Natl. Acad. Sci. USA* **99**, 8713-8718. doi:10.1073/pnas.122571799

Rosen, V. (2009). BMP2 signaling in bone development and repair. *Cytokine Growth Factor. Rev.* **20**, 475-480. doi:10.1016/j.cytogfr.2009.10.018

Rueda, E. M., Hall, B. M., Hill, M. C., Swinton, P. G., Tong, X., Martin, J. F. and Poché, R. A. (2019). The Hippo pathway blocks mammalian retinal Müller glial cell reprogramming. *Cell Rep.* **27**, 1637-1649. doi:10.1016/j.celrep.2019.04.047

Rutkovskiy, A., Stensløkken, K.-O. and Vaage, I. J. (2016). Osteoblast differentiation at a glance. *Med. Sci. Monit. Basic Res.* **22**, 95-106. doi:10.12659/MSMBR.901142

Schindelin, J., Arganda-Carreras, I., Frise, E., Kaynig, V., Longair, M., Pietzsch, T., Preibisch, S., Rueden, C., Saalfeld, S., Schmid, B. et al. (2012). Fiji: an open-source platform for biological-image analysis. *Nat. Methods* **9**, 676-682. doi:10.1038/nmeth.2019

Seo, E., Basu-Roy, U., Gunaratne, P. H., Coarfa, C., Lim, D.-S., Basilico, C. and Mansukhani, A. (2013). SOX2 regulates YAP1 to maintain stemness and determine cell fate in the Osteo-Adipo lineage. *Cell Rep.* **3**, 2075-2087. doi:10.1016/j.celrep.2013.05.029

Shrivats, A. R., McDermott, M. C. and Hollinger, J. O. (2014). Bone tissue engineering: state of the union. *Drug Discov. Today* **19**, 781-786. doi:10.1016/j.drudis.2014.04.010

Singh, S. P., Holdway, J. E. and Poss, K. D. (2012). Regeneration of amputated zebrafish fin rays from de novo osteoblasts. *Dev. Cell* **22**, 879-886. doi:10.1016/j.devcel.2012.03.006

Smith, A., Avaron, F., Guay, D., Padhi, B. K. and Akimenko, M. A. (2006). Inhibition of BMP signaling during zebrafish fin regeneration disrupts fin growth and scleroblast differentiation and function. *Dev. Biol.* **299**, 438-454. doi:10.1016/j.ydbio.2006.08.016

Sousa, S., Afonso, N., Bensimon-Brito, A., Fonseca, M., Simoes, M., Leon, J., Roehl, H., Cancela, M. L. and Jacinto, A. (2011). Differentiated skeletal cells contribute to blastema formation during zebrafish fin regeneration. *Development* **138**, 3897-3905. doi:10.1242/dev.064717

Stewart, S., Gomez, A. W., Armstrong, B. E., Henner, A. and Stankunas, K. (2014). Sequential and opposing activities of Wnt and BMP coordinate zebrafish bone regeneration. *Cell Rep.* **6**, 482-498. doi:10.1016/j.celrep.2014.01.010

Tang, Y., Rowe, R. G., Botvinick, E. L., Kurup, A., Putnam, A. J., Seiki, M., Weaver, V. M., Keller, E. T., Goldstein, S., Dai, J. et al. (2013). MT1-MMP-dependent control of skeletal stem cell commitment via a β1-Integrin/YAP/TAZ signaling axis. *Dev. Cell* **25**, 402-416. doi:10.1016/j.devcel.2013.04.011

Tu, S. and Johnson, S. L. (2011). Fate restriction in the growing and regenerating zebrafish fin. *Dev. Cell* **20**, 725-732. doi:10.1016/j.devcel.2011.04.013

Valenti, M. T., Carbonare, L. D. and Mottes, M. (2017). Osteogenic differentiation in healthy and pathological conditions. *Int. J. Mol. Sci.* **18**, 41. doi:10.3390/ijms18010041

Wehner, D. and Weidinger, G. (2015). Signaling networks organizing regenerative growth of the zebrafish fin. *Trends Genet.* **31**, 336-343. doi:10.1016/j.tig.2015.03.012

Wehner, D., Cizelsky, W., Vasudevaro, M. D., Özhan, G., Haase, C., Kagermeier-Schenk, B., Röder, A., Dorsky, R. I., Moro, E., Argenton, F. et al. (2014). Wnt/β-catenin signaling defines organizing centers that orchestrate growth and differentiation of the regenerating zebrafish caudal fin. *Cell Rep.* **6**, 467-481. doi:10.1016/j.celrep.2013.12.036

Wei, J. and Karsenty, G. (2015). An overview of the metabolic functions of osteocalcin. *Rev. Endocr. Metab. Disord.* **16**, 93-98. doi:10.1007/s11154-014-9307-7

Westerfield, M. (2000). *The Zebrafish Book. A Guide for the Laboratory use of Zebrafish (Danio rerio)*, 4th edn. Eugene: University of Oregon Press.
Wu, M., Chen, G. and Li, Y.-P. (2016). TGF-β and BMP signaling in osteoblast, skeletal development, and bone formation, homeostasis and disease. *Bone Res.* **4**, 16009. doi:10.1038/boneres.2016.9
Xiong, J., Almeida, M. and O'Brien, C. A. (2018). The YAP/TAZ transcriptional co-activators have opposing effects at different stages of osteoblast differentiation. *Bone* **112**, 1-9. doi:10.1016/j.bone.2018.04.001
Yu, F.-X. and Guan, K.-L. (2013). The Hippo pathway: regulators and regulations. *Genes Dev.* **27**, 355-371. doi:10.1101/gad.210773.112
Zhao, B., Wei, X., Li, W., Udan, R. S., Yang, Q., Kim, J., Xie, J., Ikenoue, T., Yu, J., Li, L. et al. (2007). Inactivation of YAP oncoprotein by the Hippo pathway is involved in cell contact inhibition and tissue growth control. *Genes Dev.* **21**, 2747-2761. doi:10.1101/gad.1602907
Zhao, A., Qin, H. and Fu, X. (2016). What determines the regenerative capacity in animals? *Bioscience* **66**, 735-746. doi:10.1093/biosci/biw079